View metadata, citation and similar papers at core.ac.uk

brought to you by CORE

provided by Elsevier - Publisher Connector

Available online at www.sciencedirect.com

ScienceDirect

Virology 358 (2007) 136–147

VIROLOGY

www.elsevier.com/locate/yviro

An arginine-to-proline mutation in a domain with undefined functions within the helicase protein (Nsp13) is lethal to the coronavirus infectious bronchitis virus in cultured cells

Shouguo Fang [a], Bo Chen [b], Felicia P.L. Tay [a], Beng Sern Ng [a], Ding Xing Liu [a,b,*]

[a] *Institute of Molecular and Cell Biology, 61 Biopolis Drive, Proteos, 138673 Singapore*

[b] *School of Biological Sciences, Nanyang Technological University, 60 Nanyang Drive, 637551 Singapore*

Received 5 June 2006; returned to author for revision 30 June 2006; accepted 11 August 2006

Available online 18 September 2006

Abstract

Genetic manipulation of the RNA genomes by reverse genetics is a powerful tool to study the molecular biology and pathogenesis of RNA viruses. During construction of an infectious clone from a Vero cell-adapted coronavirus infectious bronchitis virus (IBV), we found that a G–C point mutation at nucleotide position 15526, causing Arg-to-Pro mutation at amino acid position 132 of the helicase protein, is lethal to the infectivity of IBV on Vero cells. When the in vitro-synthesized full-length transcripts containing this mutation were introduced into Vero cells, no infectious virus was rescued. Upon correction of the mutation, infectious virus was recovered. Further characterization of the in vitro-synthesized full-length transcripts containing the G15526C mutation demonstrated that this mutation may block the transcription of subgenomic RNAs. Substitution mutation of the Arg132 residue to a positively charged amino acid Lys affected neither the infectivity of the in vitro-synthesized transcripts nor the growth properties of the rescued virus. However, mutation of the Arg132 residue to Leu, a conserved residue in other coronaviruses at the same position, reduced the recovery rate of the in vitro-synthesized transcripts. The recovered mutant virus showed much smaller-sized plaques. On the contrary, a G–C and a G–A point mutations at nucleotide positions 4330 and 9230, respectively, causing Glu–Gln and Gly–Glu mutations in or near the catalytic centers of the papain-like (Nsp3) and 3C-like (Nsp5) proteinases, did not show detectable detrimental effect on the rescue of infectious viruses and the infectivity of the rescued viruses.

© 2006 Elsevier Inc. All rights reserved.

Keywords: Coronavirus infectious bronchitis virus; Infectious clone; Helicase; Arginine-to-proline mutation; Infectivity

Introduction

Coronaviruses cause severe diseases affecting human and other animal species. In 2003, a novel coronavirus (SARS-CoV) was identified as the causative agent of severe acute respiratory syndrome (SARS) (Marra et al., 2003; Rota et al., 2003). The potential risk to public health posed by SARS-CoV and other coronaviruses and the lack of specific antiviral agents and vaccines have triggered a global research effort to characterize this family of viruses at the molecular and cellular levels. Major advances in studies of the biological functions of individual viral proteins and replication mechanisms are currently being made by genetic manipulation of coronaviral genomes using reverse genetics and targeted recombination approaches (Almazan et al., 2000; Casais et al., 2001, 2003, 2005; Coley et al., 2005; Hodgson et al., 2006; Koetzner et al., 1992; Masters and Rottier, 2005; Sanchez et al., 1999; Thiel et al., 2001; Youn et al., 2005a, 2005b; Yount et al., 2000, 2002, 2003, 2005).

Avian infectious bronchitis virus (IBV), a group 3 coronavirus, causes an acute and contagious disease in chickens with a significant impact on the poultry industry worldwide. IBV contains a 27.6 kb single-stranded, positive-sense RNA genome. In the virus-infected cells, six mRNA species, including the genome-length mRNA 1 and five subgenomic mRNAs (mRNA 2–6), are produced by a discontinuous RNA transcription mechanism. Each mRNA species possesses a 64 nucleotides leader sequence derived from the 5′ end of the

* Corresponding author. Institute of Molecular and Cell Biology, 61 Biopolis Drive, Proteos, 138673 Singapore.

E-mail address: dxliu@imcb.a-star.edu.sg (D.X. Liu).

0042-6822/$ - see front matter © 2006 Elsevier Inc. All rights reserved.
doi:10.1016/j.virol.2006.08.020

genome (Boursnell et al., 1987). Subgenomic mRNAs 2, 3, 4, and 6 encode the four structural proteins, i.e., spike glycoprotein (S), envelope protein (E), membrane protein (M), and nucleocapsid protein (N). The 5′ two-third region of mRNA 1 comprises two large ORFs, 1a and 1b, and encodes two polyproteins. The two polyproteins are proteolytically cleaved by two virus-encoded proteinases, the papain-like and 3C-like proteinases, into 15 functional proteins (Nsp2–Nsp16) (Lim and Liu, 1998a, 1998b; Lim et al., 2000; Liu et al., 1995, 1997, 1998; Ng and Liu, 1998, 2000, 2002; Xu et al., 2001). Compared to other coronaviruses, Nsp1 is absent in IBV but Nsp2 is considerably larger (Lim and Liu, 1998a, 1998b; Liu et al., 1995). In general, IBV shares close similarities in the genome organization, gene expression, and RNA replication with other coronaviruses but is non-infectious to human. These properties make IBV an attractive model system for studying the biology and pathogenesis of coronavirus.

In construction of an infectious IBV clone by in vitro assembly of five cloned RT-PCR fragments from a Vero cell-adapted IBV Beaudette strain, a G–C (G15526C) point mutation at nucleotide position 15,526 was found to be lethal to the infectivity of IBV on Vero cells. No infectious virus could be rescued from Vero cells electroporated with in vitro-synthesized full-length transcripts containing this mutation. As this mutation causes Arg132–Pro mutation in a domain with unknown function within the helicase protein (Nsp13), it implies that this region might play certain roles in the functionality of the helicase protein. On the contrary, a G–C (G4330C) and a G–A (G9230) point mutations at nucleotide positions 4330 and 9230, respectively, causing Glu–Gln and Gly–Glu mutations in or near the catalytic centers of the papain-like (Nsp3) and 3C-like (Nsp5) proteinases, did not impair the infectivity of the in vitro-synthesized transcripts containing these mutations. Further characterization of the in vitro-synthesized full-length transcripts containing the G15526C mutation demonstrated that this mutation blocks the transcription of subgenomic RNAs. Substitution mutation of the Arg132 residue to a positively charged amino acid (Lys) affected neither the infectivity of the in vitro-synthesized transcripts nor the growth properties of the rescued virus. However, mutation of the Arg132 residue to a Leu, which is conserved in most of other coronaviruses at the same position, reduced the viral recovery rate of the in vitro-

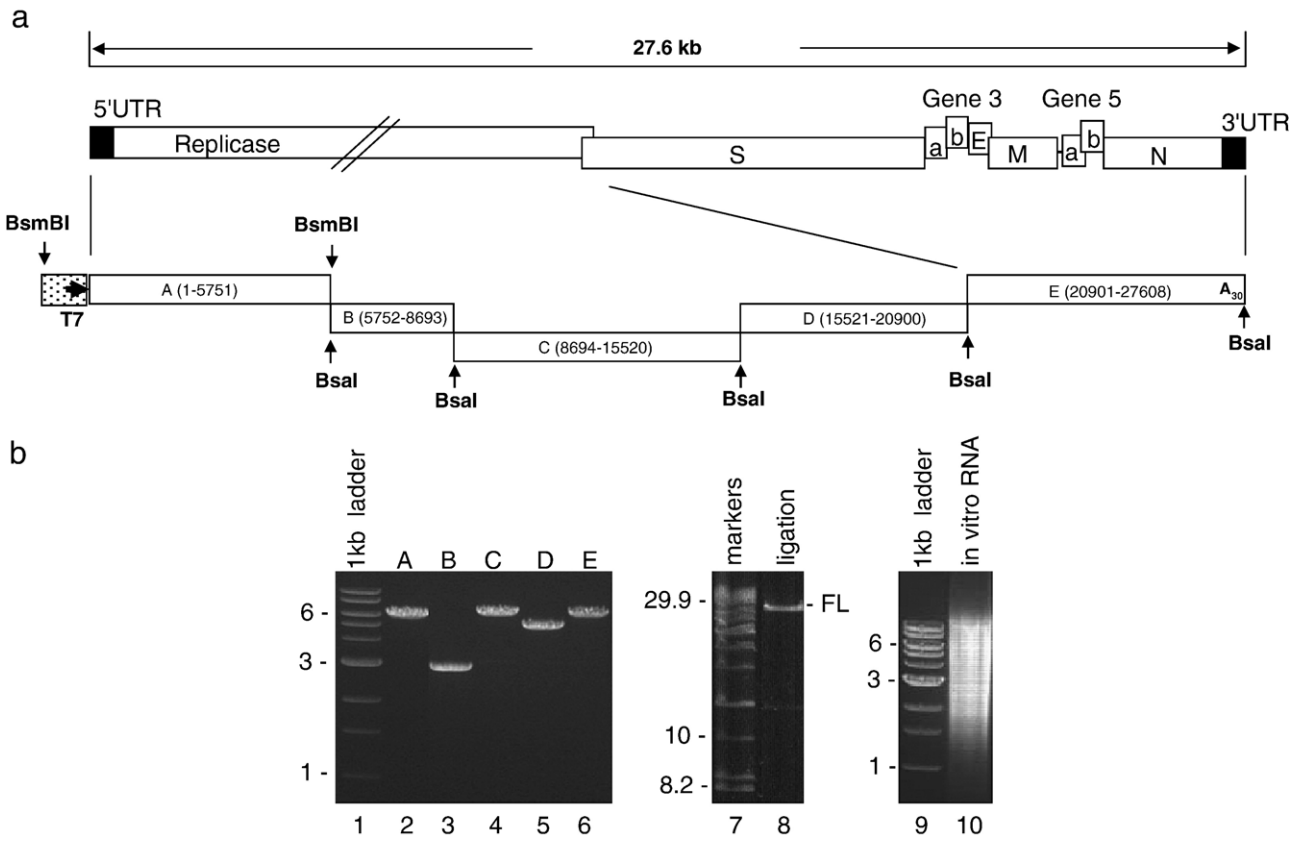

Fig. 1. In vitro assembly of full-length cDNA clone derived from a Vero cell-adapted IBV Beaudette strain. (a) Diagram of the genome organization of IBV. The regions coding for the replicase polyproteins, the structural proteins S, E, M, and N, the accessory proteins 3a, 3b, 5a, and 5b, and the 5′- and 3′-UTR are shown. Also shown are the regions of the five RT-PCR fragments, the T7 promoter at the 5′-end of fragment A, and the 30 As at the 3′-end of fragment E. (b) Preparation of the five cDNA fragments, assembly of the five fragments into a full-length cDNA clone, and in vitro transcription of the full-length transcripts. The five cDNA fragments covering IBV sequences from nucleotides 1–5751 (lane 2), 5752–8693 (lane 3), 8694–15,520 (lane 4), 15,521–20,900 (lane 5), and 20,901–27,608 (lane 6), respectively, were obtained by digestion of corresponding plasmid DNA with either *Bsm*BI or *Bsa*I, purified from agarose gel, and analyzed on a 0.8% agarose gel (lanes 2–6). Equal amounts of the purified fragments were ligated using T4 DNA ligase (lane 7) and analyzed on a 0.4% agarose gel. The in vitro assembled full-length cDNA was used as templates for generation of the full-length in vitro transcripts, which were analyzed on a 0.8% agarose gel (lane 10). Lanes 1, 7, and 9 show DNA markers, and numbers on the left indicate nucleotides in kilobases.

synthesized full-length transcripts. The mutant virus showed much smaller-sized plaques. This study reveals the essential role of a domain with previously unassigned functions within the helicase protein in coronavirus replication.

Results

Construction of a full-length cDNA clone derived from a Vero cell-adapted IBV Beaudette strain by in vitro assembly of five RT-PCR fragments

To construct a full-length IBV clone, five fragments (A to E) spanning the entire IBV genome were obtained by RT-PCR of total RNA extracted from Vero cells infected with a Vero cell-adapted IBV Beaudette strain (p65) (Shen et al., 2003, 2004; Fang et al., 2005). To facilitate the assembly of the full-length cDNA in vitro, restriction sites for either *Bsm*BI or *Bsa*I were introduced into both the 5′ and 3′ ends of the fragments (Fig. 1a). In fragment A, a 19-nucleotide sequence corresponding to the T7 RNA promoter (Table 1) was inserted into the 5′ end of the IBV genome to facilitate in vitro transcription using the T7 polymerase (Fig. 1a). The primers used to amplify these fragments are listed in Table 1. The PCR products were purified from agarose gel and cloned into either pCR-XL-TOPO (Invitrogen) or pGEM-T Easy (Promage) vectors. For the convenience of digestion using the restriction enzyme *Bsm*BI, the *Nhe*I- and *Eco*RI-digested fragment A was subcloned into pKT0 which contains a *Bsm*BI site 400 bp upstream of the T7 promoter sequence (Fig. 1a). Two to three independent clones for each construct were selected for sequencing. The complete sequences of the five fragments, determined by automated nucleotide sequencing, are summarized in Table 2.

The five fragments were then prepared by digestion of the corresponding constructs with either *Bsm*BI or *Bsa*I and purified (Fig. 1b, lanes 2–6). The full-length clone was made by ligation of the purified fragments in vitro (Fig. 1b, lane 8) and used as the template for in vitro transcription. The full-length in vitro-synthesized transcripts were generated using the mMessage mMachine T7 kit (Ambion, Austin, Tex) (Fig. 1b, lane 10). As coronavirus N gene transcripts were shown to enhance the recovery of the rescued virus from the in vitro-synthesized full-length transcripts (Casais et al., 2001; Youn et al., 2005a, 2005b; Yount et al., 2000, 2002), the N transcripts were generated from a linearized pKT0-IBVN construct containing IBV N gene and the 3′-UTR region. The full-length transcripts together with the N transcripts were introduced into Vero cells by electroporation. However, it was consistently observed that no infectious virus could be recovered from cells transfected with the full-length transcripts together with the N transcripts.

Table 2
Comparison of IBV sequences between Vero cell-adapted strain (p65) and the cloned fragments

Position (nt)	p65		Clone	
	nt	aa	nt	aa
Nsp2 (p87)				
2015	A	D	G	**G**[a]
Nsp3 (p195)				
4330	G	E	C	**Q**
4481	C	T	A	**N**
Nsp5 (3CLP)				
9230	G	G	A	**E**
9701–3	-GTG	-G	GTG	G[b]
Nsp6				
10,253	G	S	A	N
10,540	G	D	A	**N**
10,594	G	E	A	**K**
Nsp8 (p24)				
10,942	A	T	C	P
11,362	C	H	T	**Y**
Nsp13 (helicase)				
15,526	G	R	C	**P**
Nsp14 (p58)				
17,033	C	D	T	D
17,674	C	S	T	**L**
18,195	T	Y	C	**H**
18,430	C	S	T	F
N				
26,398	G	A	T	**S**

[a] Unique mutations found only in the cloned fragments.
[b] Same as the published sequences but different from p65.

Rescue of infectious virus by correction of a point mutation (G15526C) located in a domain with unknown function within the helicase protein (Nsp13)

Sequencing comparison of the five fragments with the Vero cell-adapted IBV strain (p65, accession no. DQ001339) shows nucleotide changes at 16 positions (Table 2). Among them, 11

Table 1
Primers used to construct the full-length IBV clone

Clone	Primer	Nucleotide sequence	Location
A	T7-IBV	5′-CGCTAGCTAATACGACTCACTATAGGACTTAAGATAGATATTAATA-3′	1–20
	IBV-5753R	5′-CGGGATC**CGTCTC**GCGACAACACTCTTAAC-3′	5737–5753
B	IBV-5748F	5′-ATTAT**GGTCTC**TGTCGCTAGCTATAAGACCG-3′	5748–5768
	IBV-8694R	5′-G**GGTCTC**GGCCTCAAATTTATCACCTATC-3′	8673–8694
C	IBV-8689F	5′-CGGGATCC**GGTCTC**GAGGCCTACCTTTCAGCG-3′	8689–8706
	IBV-15532R	5′-GCAAAA**GGTCTC**AATGAATCAC-3′	15,511–15,532
D	IBV-15511F	5′-CGGGATCCGTGATTCATT**GAGACC**TTTTGC-3′	15,511–15,532
	IBV-20930R	5′-ACACCTGCAGATGTAACATC-3′	20,911–20,930
E	IBV-20887F	5′-GTTTACACCTCTAAT**GAGACC**ATAG-3′	20,887–20,911
	IBV-27608R	5′-GGAATTC**GGTCTC**G(T)$_{30}$TGCTCTAACTCTATACTAGC-3′	27,589–27,608

caused unique amino acid changes (Table 2). To assess the deleterious effects of these mutations on the infectivity of the full-length clone, correction of some of the mutations was carried out by site-directed mutagenesis. Three point mutations, G4330C, G9230A, and G15526C, were chosen based on the fact that they are located either in or near the catalytic centers of the two viral proteinases or in a region of the RNA helicase protein with undefined functions. Four full-length cDNA clones either with correction of the mutations at all three positions (rIBV) or combination of two positions (e.g., G4330C containing G–C mutation at nucleotide position 4330 but without mutations at the other two positions) were constructed. RNA transcripts generated from the four full-length cDNA clones were introduced into Vero cells together with the N transcripts by electroporation. At 2 days post-electroporation, a typical CPE of the Vero cell-adapted IBV, the formation of giant syncytial cells (Fang et al., 2005), was observed in cells transfected with transcripts generated from cDNA clones rIBV, G4330C, and G9230A. CPE was extended to almost the whole monolayers at 3 days post-electroporation (Fig. 2a). No CPE was observed in cells transfected with transcripts generated from clone G15526C (Fig. 2a).

RT-PCR analysis of the subgenomic mRNA 5 was performed to confirm if CPE observed is caused by the replication of IBV. Sequencing of the RT-PCR fragment generated from cells transfected with rIBV showed correct sequence in the leader/body junction region of the subgenomic mRNA (Fig. 2b). Further sequencing of the RT-PCR fragments covering regions with unique amino acid mutations confirmed the recovery of IBV (rIBV) from the in vitro-synthesized full-length transcripts.

Characterization of the rescued IBV virus (rIBV)

Compared to the parent IBV strains, rIBV contains 8 amino acid mutations (Table 2). To test if these mutations may affect the growth properties and genetic stability of the rescued virus, rIBV was propagated on Vero cells for 5 passages, and the plaque sizes and growth kinetics were determined and compared with wild type IBV p65. In cells infected with

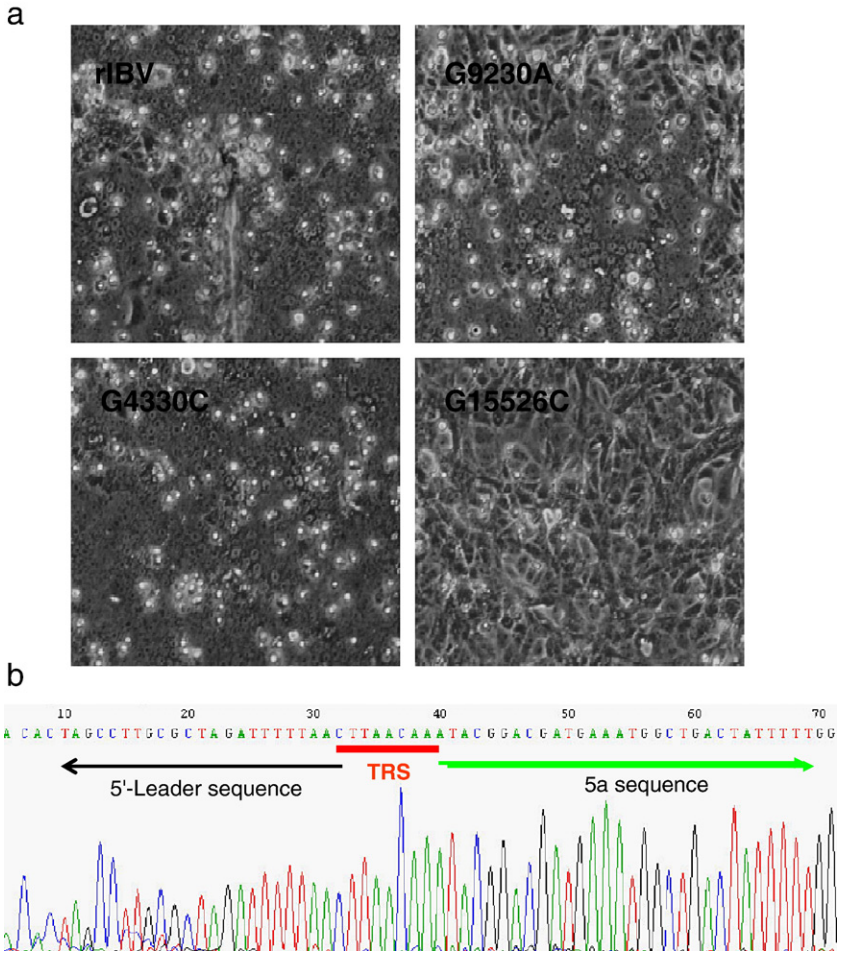

Fig. 2. Recovery of infectious viruses from cells electroporated with in vitro-synthesized full-length transcripts. (a) Vero cells electroporated with in vitro-synthesized transcripts derived from the in vitro assembled full-length clones with or without a point mutation at one of the three positions (G4330C, G9230A, or G15526C). Images were taken at 3 days post-electroporation. (b) Nucleotide sequencing of the leader/body junction of the subgenomic mRNA 5. Total RNA was prepared from Vero cells infected with the recombinant virus rescued from the in vitro-synthesized full-length transcripts 24 h post-infection. The 5′ 400-nucleotide region of the subgenomic mRNA 5 was amplified by RT-PCR and sequenced by automated nucleotide sequencing. The 70 nucleotides flanking the transcription regulatory sequence (TRS) for mRNA 5 are shown.

rIBV, the average plague size is 0.56±0.028 mm, which is slightly smaller than the average plaque size of 0.68±0.034 mm in cells infected with wild type IBV (Fig. 3a). Analysis of the growth curves demonstrated that rIBV exhibited very similar growth properties as the wild type virus (Fig. 3a).

Further characterization of rIBV was subsequently carried out by analysis of viral RNAs and structural proteins. Northern blot and Western blot analyses showed the detection of very similar amounts of viral RNAs (Fig. 3b), and S, N, and M proteins (Fig. 3c) in cells infected with wild type and rIBV, respectively, at 24 h post-infection. When probing with anti-N protein antibodies, other species migrating faster than the full-length products on SDS-PAGE were also observed (Fig. 3c). They may represent premature termination and cleavage products of N protein (unpublished observation). It was also noted that variable amounts of these species were detected in cells infected with wild type and rIBV (Fig. 3c). The significance of these variations is unclear at the moment. Taken together, these results confirm that rIBV is stable and possesses very similar growth properties as wild type IBV.

Absence of subgenomic RNA transcription in cells transfected with G15526C mutant transcripts

As no infectious virus was recovered from cells transfected with G15526C mutant transcripts, RT-PCR amplification of the negative strand RNA was performed to check if RNA replication occurred in these transfected cells. Total RNA was extracted from Vero cells transfected with wild type and G15526C mutant transcripts at 24 and 48 h post-electroporation, respectively. Reverse transcription was performed by using equal amount of RNA and the sense-primer IBV14931-F (5′-$_{14,931}$GCTTATCCACTAGTACATC$_{14,949}$-3′), and PCR was carried out by using the sense-primer IBV14931-F and the antisense-primer IBV15600-R (5′-$_{15,600}$CTTCTCGCACTTCTGCACTAGCA$_{15,578}$-3′). If replication of viral RNA occurred, a 670 bp PCR fragment would be expected. As shown in Fig. 4a, RT-PCR fragments amplified from negative strand RNA templates were obtained from cells transfected with both wild type (lanes 2 and 4) and the mutant transcripts (lanes 3 and 5). Sequencing of the PCR fragments confirmed that they represent the correct sequences. As a negative control, the in vitro-synthesized transcripts were mixed with total RNA extracted from normal Vero cells and were used as a template for RT-PCR. No RT-PCR fragment was detected (Fig. 4a, lane 6), confirming that the detection of negative strand RNA from cells transfected with mutant transcripts is due to the replication of viral RNA. Further quantitation of the negative strand RNA transcription in cells transfected with wild type and G15526C mutant transcripts was carried out by real-time PCR. At 24 and 48 h post-electroporation, transcription of the negative RNA in cells electroporated with wild type transcripts was 24.76- and 945.54-fold, respectively, higher than that in cells electroporated with the G15526C mutant transcripts. These results confirm that transcription of the negative strand RNA has taken place in cells transfected with the mutant transcripts, but with much lower efficiency.

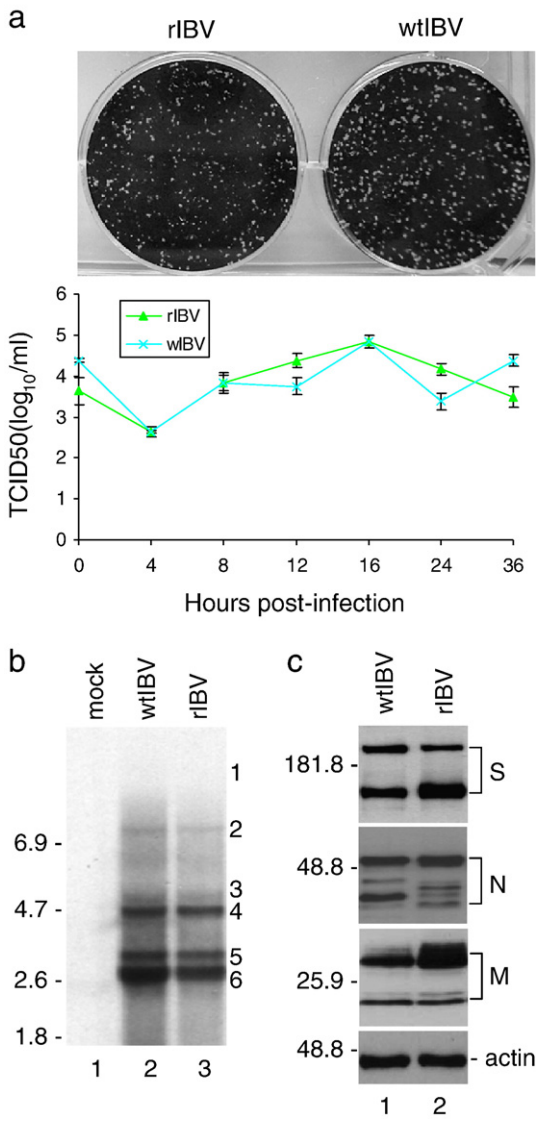

Fig. 3. Analysis of the growth properties of wild type (p65) and rIBV. (a) Plague sizes and one-step growth curves of wild type and rIBV. Monolayers of Vero cells on a 6-well plate were infected with 100 μl of 1000-fold diluted virus stock and cultured in the presence of 0.5% carboxymethy cellulose at 37 °C for 3 days. The cells were fixed and stained with 0.1% toluidine. To determine the one-step growth curves of wild type and rIBV, Vero cells were infected with the viruses and harvested at 0, 4, 8, 12, 16, 24, and 36 h post-inoculation, respectively. Viral stocks were prepared by freezing/thawing of the cells three times, and TCID50 of each viral stock was determined by infecting five wells of Vero cells on 96-well plates in triplicate with 10-fold serial dilution of each viral stock. Error bar shows standard error of the mean. (b) Northern blot analysis of the genomic and subgenomic RNAs in cells infected with wild type and rIBV. Ten micrograms of total RNA extracted from Vero cells infected with wild type and rIBV, respectively, was separated on 1% agarose gel and transferred to a Hybond N+ membrane. Viral RNAs were probed with a Dig-labeled DNA probe corresponding to the 3-end 680 nucleotides of the IBV genome. Total RNA extracted from mock-infected cells was included as negative control. Numbers on the left indicate nucleotides in kilobase, and numbers on the right indicate the genomic and subgenomic RNA species of IBV. (c) Western blot analysis of viral protein expression in cells infected with wild type and rIBV. Vero cells infected with wild type (lane 1) and rIBV (lane 2) were harvested, lysates prepared and separated on SDS-10% polyacrylamide gel. The expression of S, N, and M proteins was analyzed by Western blot with polyclonal anti-S, anti-N, and anti-M antibodies, respectively. The same membrane was also probed with anti-actin antibody as a loading control. Numbers on the left indicate molecular masses in kilodaltons.

RT-PCR amplification of subgenomic mRNAs was carried out to check if a low level of subgenomic mRNA synthesis could occur in cells transfected with the mutant transcripts. Total RNA prepared from the transfected cells 2 days post-electroporation was used in the RT reaction with the sense-primer IBV-leader ($5'$-$_{26}$CTATTACACTAGCCTTGCGCT$_{46}$-$3'$) for the detection of negative-stranded sgRNA, and the antisense-primer IBV24803-R ($5'$-$_{24,803}$CTCTGGATCCAATAACC-TAC$_{24,784}$-$3'$) for the detection of positive-stranded sgRNA. The two primers were then used for PCR. If transcription of subgenomic mRNAs did occur, a 415 bp PCR product corresponding to the $5'$-terminal region of the subgenomic mRNA 4 and a 1010 bp fragment corresponding to the $5'$-terminal region of the subgenomic mRNA 3 would be expected. As shown in Fig. 4b, a dominant 415 bp band and a weak 1010 bp band were observed in cells electroporated with wild type full-length transcripts at 2 days post-electroporation (lanes 2 and 5). Sequencing of the PCR fragments confirmed that they represent the correct sequences of the corresponding regions of the subgenomic mRNAs 3 and 4, respectively. However, the same PCR products were not detected in cells electroporated with the mutant transcripts (Fig. 4b, lanes 3 and 6). As a negative control, the amplified fragments were not detected in cells without electroporation (Fig. 4b, lane 4). The failure to detect both negative- and positive-stranded sgRNAs in cells transfected with the mutant transcripts show that the G15526C mutation leads to the disruption of subgenomic RNA transcription.

To further demonstrate that the failure to rescue infectious virus from the G15526C mutant transcripts is due to a defect in subgenomic RNA transcription, the full-length clones with and without the G15526C mutation were used to generate recombinant IBV expressing the enhanced green fluorescent protein (EGFP) by replacing the 5a gene with EGFP. Full-length transcripts containing EGFP were synthesized in vitro and introduced into Vero cells together with the N transcripts by electroporation. At 2 days post-electroporation, single CPE with the expression of EGFP was observed in cells transfected with the full-length transcripts without the G15526C mutation

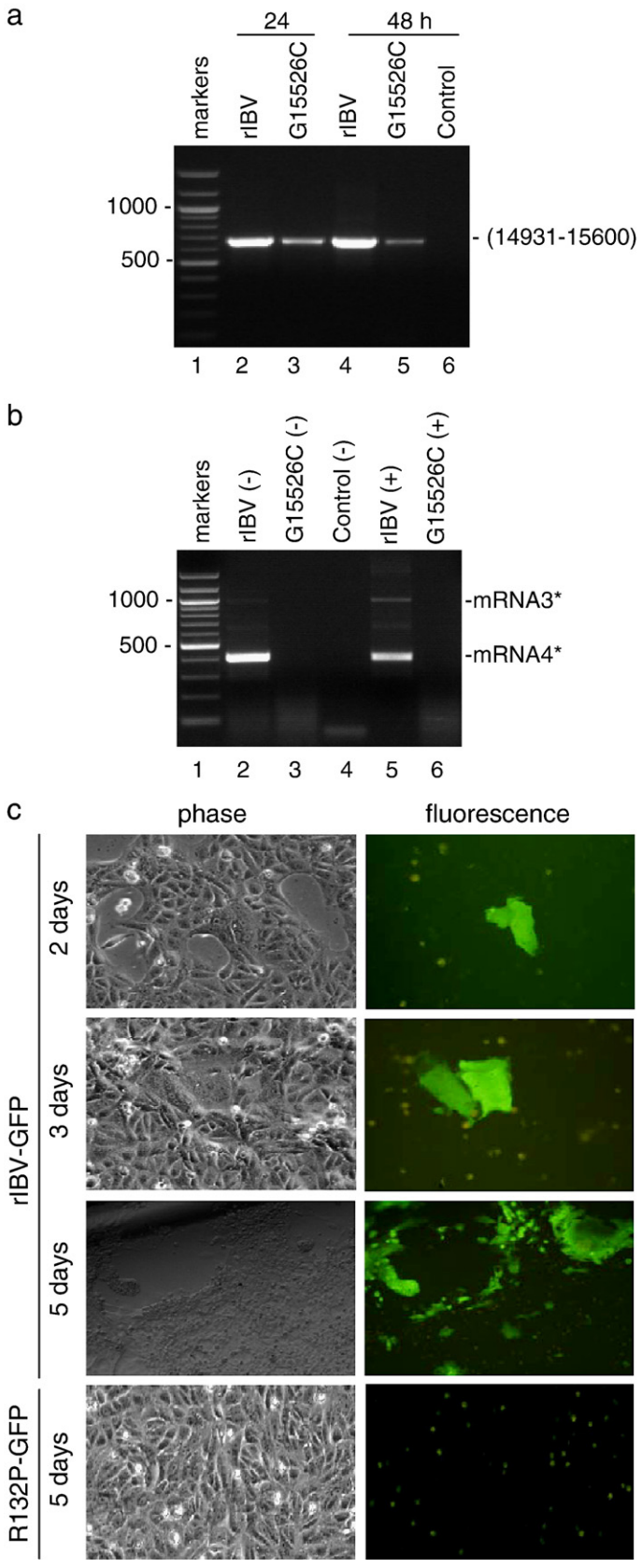

Fig. 4. Analysis of RNA replication in cells electroporated with G15526C mutant transcripts. (a) Detection of negative strand RNA synthesis in cells electroporated with wild type (lanes 2 and 4) and G15526C mutant (lanes 3 and 5) transcripts. Total RNA was prepared from Vero cells electroporated with in vitro-synthesized full-length transcripts at 24 and 48 h post-electroporation, respectively. Region corresponding to nucleotides 14,931–15,600 of the negative (−) sense IBV genomic RNA was amplified by RT-PCR and analyzed on 1.2% agarose gel. Lane 1 shows DNA markers, and lane 6 shows negative control. Numbers on the left indicate nucleotides in bases. (b) Detection of the negative and positive strand subgenomic RNA synthesis in cells electroporated with wild type (lanes 2 and 5) and G15526C mutant (lanes 3 and 6) transcripts. Total RNA was prepared from Vero cells electroporated with in vitro-synthesized full-length transcripts 2 days post-electroporation. Regions corresponding to the $5'$-terminal 415 and 1010 nucleotides of the subgenomic mRNA 4 and 3, respectively, were amplified by RT-PCR and analyzed on 1.2% agarose gel. Lane 1 shows DNA markers, and lane 4 shows negative cell control. Numbers on the left indicate the length of DNA in bases. (c) Construction of a recombinant IBV expressing EGFP and further analysis of the effect of G15526C mutation on subgenomic transcription using the recombinant virus. Vero cells electroporated with in vitro-synthesized transcripts derived from the in vitro assembled full-length clones containing EGFP either with or without G15526C mutation. Phase-contrast and fluorescent images were taken 2, 3, and 5 days post-electroporation, respectively.

(Fig. 4c). Gradually increased CPE and fluorescent cells were observed from 3 to 5 days post-electroporation (Fig. 4c). At 5 days post-electroporation, CPE and fluorescent cells were extended to almost the whole monolayer (Fig. 4c). However, it was consistently observed that much less infectious virus was recovered from cells transfected with this construct. Furthermore, the recombinant virus rapidly lost infectivity when passaged on Vero cells; the recovered virus maintains minor infectivity only for one passage. In cells transfected with the full-length transcripts containing the G15526C mutation, neither CPE nor cells expressing EGFP were observed (Fig. 4c), demonstrating that G15526C mutation led to total demolition of the EGFP expression. As EGFP could be expressed only if subgenomic RNAs were synthesized but can be observed even if a single cell was transfected and expressed the protein to a certain level, these results reinforce the conclusion that the G15526C mutation blocks subgenomic RNA transcription.

Mutational analysis of the R132 residue of the helicase protein

G15526C mutation resulted in the substitution mutation of the R132 with a Pro (R132P) of the helicase protein. Sequence comparison of the IBV helicase protein with other known coronaviruses showed that R132 residue is located adjacent to a conserved motif (Fig. 5a). In all sequenced coronaviruses, only IBV has a charged amino acid (R132) at this position (Fig. 5a). To assess if a positive charge amino acid at this position is essential for the function of the protein, mutation of R132 to a Lys (R132K) was carried out. Meanwhile, a conserved Leu residue (Ile in the case of TGEV) was found at this position in all other coronaviruses, mutation of R132 to a Leu (R132L) was also included.

In vitro full-length transcripts containing the R132K and R132L mutations were electroporated into Vero cells. As shown in Fig. 5b, transcripts generated from wild type (R132) and R132K mutant constructs showed very similar infectivity after introduction into Vero cells. Typical CPE was observed in large areas of the monolayers at 3 days post-electroporation (Fig. 5b), and recombinant viruses were recovered. However, R132L transcripts were found to be less infectious. In cells electroporated with transcripts generated from this mutant, typical CPE was observed in much restricted areas of the monolayer at 3 days post-electroporation (Fig. 5b).

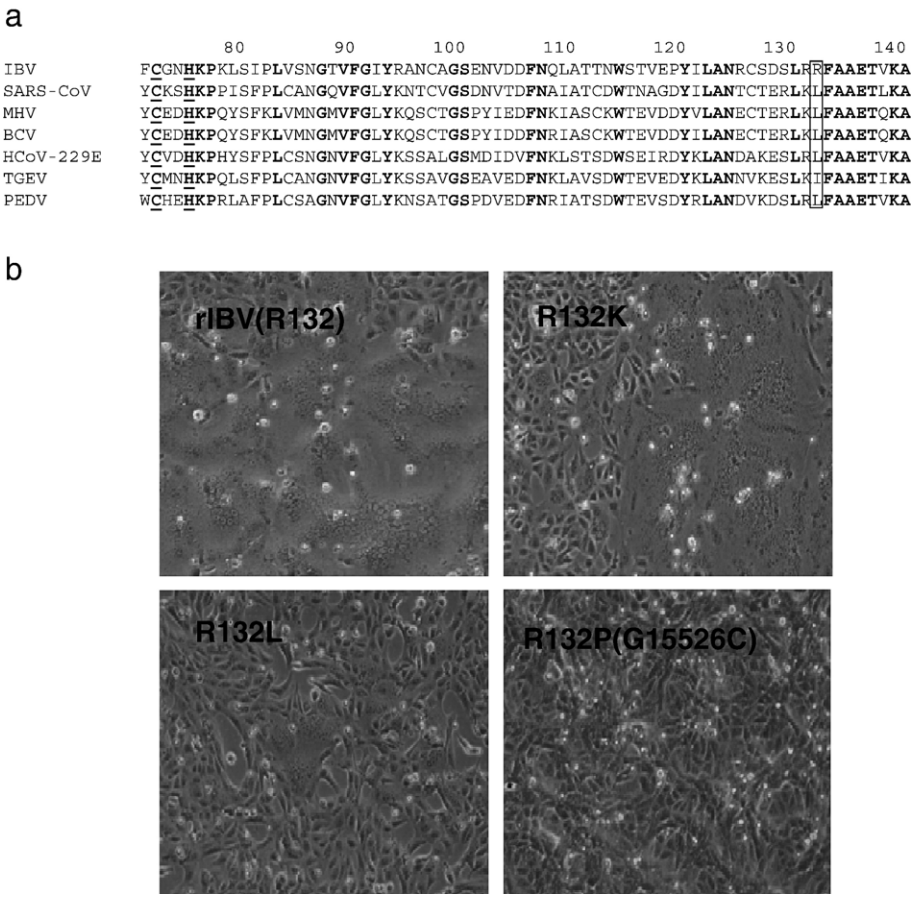

Fig. 5. Mutational analysis of the R132 residue of the helicase protein. (a) Sequence comparison of the region between amino acids 70 and 140 of helicase proteins from seven different coronaviruses. The identical amino acids are shown in bold, and the last Cys/His residues of the zinc-binding domain are shown in bold and underlined. Also shown are the R132 residue in IBV and the equivalent amino acids in other coronaviruses (boxed). (b) Vero cells electroporated with in vitro-synthesized transcripts derived from wild type recombinant IBV (rIBV), R132K, R132L, and R132P (G15526C) constructs. Phase-contrast images were taken 3 days post-electroporation.

Genetic stability and growth kinetics of R132K and R132L mutant viruses

The growth properties of the R132K and R132L mutant viruses on Vero cells were tested by analysis of plaque sizes and growth curves of passage 5 mutant viruses. Compared to cells infected with wild type recombinant virus (average plaques size is 0.56±0.028), plaques with similar size were observed in cells infected with the R132K mutant virus (Fig. 6a). The average plaque size in cells infected with R132K mutant virus is 0.59±0.029 mm. In cells infected with the R132L mutant virus, much smaller-sized plaques were observed (Fig. 6a). The average plaque size in cells infected with this mutant virus is 0.24±0.017 mm. However, analysis of the growth curves of wild type and mutant viruses demonstrated that the mutant viruses exhibited very similar, or even better, growth properties as the wild type recombinant virus (Fig. 6a).

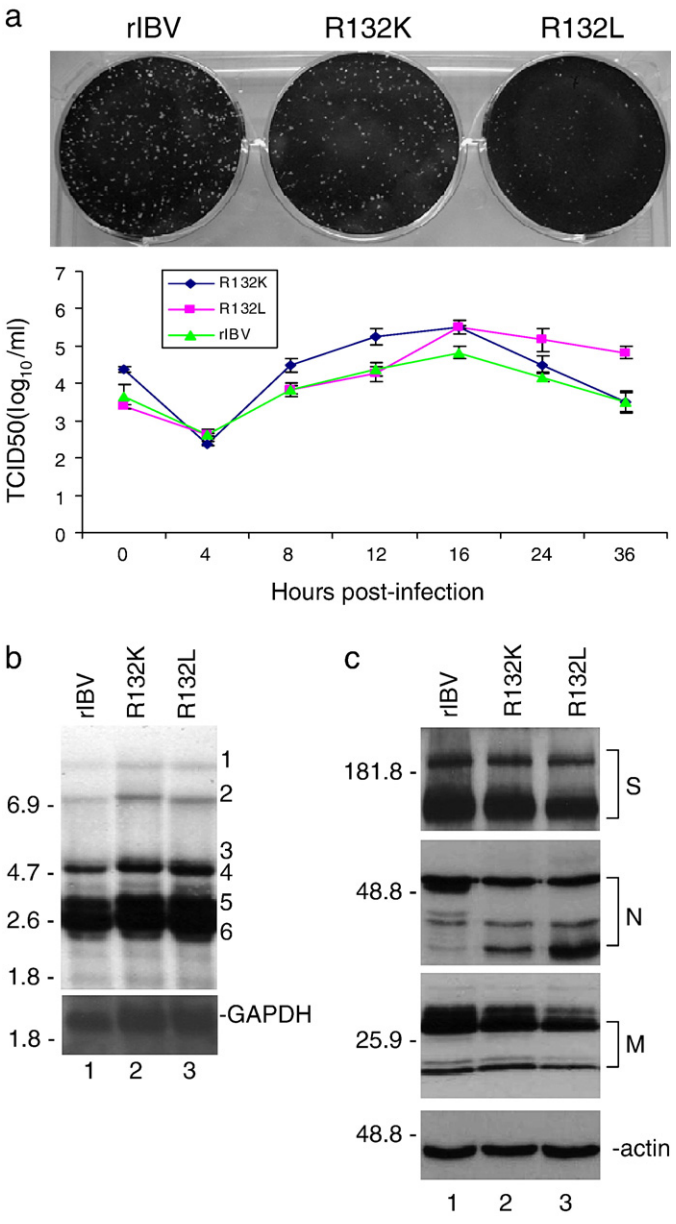

The R132K and R132L mutant viruses were subsequently characterized by analysis of viral RNAs and structural proteins. Northern blot analysis showed the detection of very similar amounts of genomic and subgenomic RNAs in cells infected with rIBV and the two mutant viruses at 24 h post-infection (Fig. 6b). Similarly, Western blot analysis of cells infected with rIBV, R132K, and R132L mutant viruses showed that similar amounts of S, N, and M proteins were detected at 24 h post-infection (Fig. 6c, lanes 1–3). When probing with anti-N protein antibodies, other species migrating faster than the full-length products on SDS-PAGE were also observed (Fig. 6c). They may represent premature termination and cleavage products of N protein (unpublished observation). It was also noted that variable amounts of these species were detected in cells infected with wild type and different mutants (Fig. 6c).

The genetic stability of R132K and R132L mutant viruses was tested by propagation of the viruses on Vero cells for 5 passages. Sequencing analysis of the fifth passages of the two mutant viruses showed that the mutations are stable. No reversion to the original sequences or mutation to other nucleotides was found in the position.

Discussion

In vitro assembly of full-length coronavirus clones, generation of full-length transcripts in vitro using a bacteriophage DNA-dependent RNA polymerase, and recovery of infectious viruses by introduction of the in vitro-synthesized transcripts into cells, first used by Yount et al. (2000), are a rapid and reliable approach to construct infectious clones from large RNA viruses. It has been successfully used to construct infectious

Fig. 6. Analysis of the growth properties of rIBV, R132K, and R132L mutant viruses. (a) Plague sizes and one-step growth curves of rIBV, R132K, and R132 mutant viruses. Monolayers of Vero cells on a 6-well plate were infected with 100 μl of 100-fold diluted virus stock and cultured in the presence of 0.5% carboxymethy cellulose at 37 °C for 3 days. The cells were fixed and stained with 0.1% toluidine. To determine the one-step growth curves of rIBV, R132K, and R132L mutant viruses, Vero cells were infected with the viruses and harvested at 0, 4, 8, 12, 16, 24, and 36 h post-inoculation, respectively. Viral stocks were prepared by freezing/thawing of the cells three times, and TCID50 of each viral stock was determined by infecting five wells of Vero cells on 96-well plates in triplicate with 10-fold serial dilution of each viral stock. Error bar shows standard error of the mean. (b) Northern blot analysis of the genomic and subgenomic RNAs in cells infected with rIBV, R132K, and R132L mutant viruses. Ten micrograms of total RNA extracted from Vero cells infected with rIBV, R132K, and R132L mutant viruses, respectively, was separated on 1% agarose gel and transferred to a Hybond N+ membrane. Viral RNAs were probed with a Dig-labeled DNA probe corresponding to the 3-end 680 nucleotides of the IBV genome. Numbers on the left indicate nucleotides in kilobase, and numbers on the right indicate the genomic and subgenomic RNA species of IBV. (c) Western blot analysis of viral protein expression in cells infected with wild type and R132 mutant viruses. Vero cells infected with wild type recombinant IBV (lane 1), R132K (lane 2), and R132L (lane 3) were harvested, lysates prepared, and separated on SDS-10% polyacrylamide gel. The expression of S, N, and M proteins was analyzed by Western blot with polyclonal anti-S, anti-N, and anti-M antibodies, respectively. The same membrane was also probed with anti-actin antibody as a loading control. Numbers on the left indicate molecular masses in kilodaltons.

clones for several coronaviruses, including transmissible gastroenteritis virus (TGEV), mouse hepatitis virus (MHV), SARS-CoV, and IBV (Youn et al., 2005a, 2005b; Yount et al., 2000, 2003). In the process of developing an infectious IBV clone from a Vero cell-adapted IBV Beaudette strain using this approach, a G–C point mutation at nucleotide position 15,526 was found to be lethal to the infectivity of the in vitro-synthesized full-length transcripts on Vero cells. No infectious virus could be rescued from Vero cells electroporated with transcripts containing this mutation. This mutation causes Arg132–Pro substitution in a domain within the helicase protein (Nsp13) with undefined functions, indicating that this domain may be essential for the functionality of the helicase protein.

Multiple enzymatic activities have been assigned to the Nsp13 helicase protein. These include RNA and DNA duplex-unwinding activities, NTPase and dNTPase activities, and an RNA 5′-triphosphatase activity that might be involved in the formation of the 5′-cap structure of viral RNAs (Ivanov et al., 2004). The protein is comprised of two domains: a putative N-terminal zinc binding domain, which spans the N-terminal region of the protein from approximately amino acids 1 to 77, and a C-terminal helicase domain covering the C-terminal part of the protein from amino acids 279 to the C-terminal end (Ivanov et al., 2004). A Ser–Pro substitution located immediately downstream of the putative zinc binding domain of Nsp10, the equivalent RNA helicase protein in equine arteritis virus (EAV), caused defect in subgenomic mRNA transcription (van Dinten et al., 1997, 2000). More detailed analysis of the zinc binding domain of Nsp10 from EAV and Nsp13 from human coronavirus 229E by mutagenesis studies showed that this domain could modulate the enzymatic activities of the helicase domain (Seybert et al., 2005). Through this regulatory role and some yet to be discovered mechanisms, the zinc binding domain is shown to be critically involved in the replication and transcription of coronavirus RNA.

In this study, introduction of the in vitro-synthesized full-length transcripts containing the G15526C (R132P) mutation was shown to be totally defective in subgenomic RNA transcription, a phenotype similar to, but appears to be much more severe than, the Ser–Pro mutation in EAV (van Dinten et al., 1997, 2000). Mutation of the Arg132 residue to a positively charged amino acid (Lys) does not affect the infectivity of the in vitro-synthesized transcripts as well as the growth properties of the rescued virus. However, mutation of the Arg132 residue to Leu, a conserved residue at the same position in most of other known coronaviruses, impaired the recovery rate of the in vitro-synthesized transcripts. The recovered mutant virus showed much smaller-sized plaques. The R132 residue is located 57 amino acids downstream of the last His (H75) residue in the putative zinc binding domain (Fig. 5a) and 147 amino acids upstream of the helicase motif 1 (Seybert et al., 2005). So far, no functional domain has been found in this region of the helicase protein.

Why the R132P substitution, located outside of the two functional domains of the helicase protein, shows severe phenotypic defect in subgenomic RNA transcription and the infectivity of IBV is not clear at the moment. Three possibilities were considered. First, R132 may be part of the N-terminal zinc binding domain. As no studies have been attempted to define the boundary of the two domains, it is not even certain that an independent domain with unique function may exist in this region. R132P mutant virus shares certain phenotypic similarity to the Ser–Pro mutant EAV, such as the absence of subgenomic mRNA transcription (van Dinten et al., 1997, 2000), suggesting that the two mutations might disrupt a similar function of the helicase protein. However, as biochemical characterization of the effect of R132P mutation on the enzymatic activities of IBV Nsp13 helicase protein is currently lacking, it would be difficult to draw a conclusion that the two mutants share mechanistically similar characteristics. Second, R132 is located in a region with a high degree of amino acid conservation in all known coronaviruses. Since the main defect of R132P mutant virus is in the subgenomic RNA transcription, one possibility is that this region may be involved in the subgenomic RNA synthesis by interacting with host or other viral functional proteins. Alternatively, as a positively charged amino acid is required to maintain the full function of the protein, it would be possible that this region may be involved in binding of the helicase protein to viral RNA during RNA replication and transcription. Finally, mutation to a Pro would lead to the disruption of the three dimensional structures of the two domains. Biochemical characterization of the involvement of this region in the enzymatic activities of the protein and determination of its three dimensional structures are underway to address these possibilities.

The G433C (E–Q) point mutation near the catalytic center of the PLP domain in Nsp3 affects neither the recovery of infectious virus from the full-length synthesized in vitro transcripts nor the infectivity of the rescued virus. Similarly, efficient recovery of infectious virus from the in vitro transcripts containing the G9230A (G–E) point mutation in the 3CLP was obtained. The two mutant viruses are genetically stable and show similar growth properties with the wild type recombinant virus. Even though the two mutations are located in or near the catalytic centers of the two viral proteinases, the mutations did not alter their enzymatic activities. This relatively high degree of tolerance to mutations in non-essential regions of important functional proteins would minimize the occurrence of lethal mutations during the replication cycles of RNA viruses and increase the adaptability of these viruses to a changed environment.

Materials and methods

Cells and virus

Vero cells were cultured at 37 °C in minimal essential medium (MEM) supplemented with 10% fetal bovine serum (FBS), penicillin (100 units/ml), and streptomycin (100 μg/ml). A Vero cell-adapted IBV Beaudette strain (65 passages on Vero cells (p65)) (Shen et al., 2003, 2004; Fang et al., 2005) was propagated in Vero cells in FBS-free MEM.

Reverse transcription (RT)-polymerase chain reaction (PCR), cloning, and sequencing

Five fragments spanning the entire IBV genome were obtained by RT-PCR from Vero cells infected with the Vero cell-adapted IBV p65 at a multiplicity of approximately 1. Briefly, total cellular RNA was extracted from the infected Vero cells with TRI Reagent (Molecular Research Center, Inc.), according to the manufacturer's instructions. Reverse transcription was performed with Expand Reverse Transcriptase (Roche) using reverse primers IBV-5753R, IBV-8694R, IBV-15532R, IBV-20930R, and IBV-27608R (Table 1). Each cDNA fragment was amplified from RT products by PCR using KOD Hot Start DNA polymerase according to the manufacturer's instructions (Novagen). The PCR products were purified from agarose gels and cloned into pCR-XL-TOPO (Invitrogen) or pGEM-T Easy (Promage) vectors. Subsequently, fragment A was removed from pCR-XL-TOPO by digestion with *Nhe*I and *Eco*RI and subcloned into pKT0 vector.

Two to three independent clones of each fragment were selected and sequenced by automated sequencing using specific primers and the ABI dye termination sequencing method. Sequence comparison, assembly, and analysis were performed by using BLAST and DNA STAR software.

PCR mutagenesis

Mutations were introduced into the corresponding fragments by using QuickChange site-directed mutagenesis kit (Stratagene) and confirmed by sequencing of the whole fragments.

In vitro assembly of full-length cDNA clones

Plasmids were digested with either *Bsm*BI (fragment A) or *Bsa*I (fragments B, C, D, and E). The digested plasmids were separated on 0.8% agarose gels containing crystal violet. Bands corresponding to each of the fragments were cut from the gels and purified with QIAquick gel extraction kit (QIAGEN Inc.).

Fragments A and B, and fragments C, D, and E were first ligated with T4 DNA ligase at 4 °C overnight. The two reaction mixtures were then mixed and further ligated at 4 °C overnight. The final ligation products were extracted with phenol/chloroform/isoamyl alcohol (25:24:1), precipitated with ethanol, and detected by electrophoresis on 0.4% agarose gels.

In vitro transcription and electroporation

Full-length transcripts were generated in vitro using the mMessage mMachine T7 kit (Ambion, Austin, TX) according to the manufacturer's instructions with certain modifications. Briefly, 30 μl of transcription reaction with a 1:1 ratio of GTP to cap analog was sequentially incubated at 40.5 °C for 25 min, 37.5 °C for 50 min, 40.5 °C 25 min and 37.5 °C for 20 min.

The N transcripts were generated by using a linearized pKTO-IBVN containing IBV N gene and the 3′-UTR region as templates. A 1:2 ratio of GTP to cap analog was used for the transcription of IBV N gene.

Introduction of in vitro-synthesized transcripts into Vero cells by electroporation

The in vitro-synthesized full-length and N transcripts were treated with DNaseI and purified with phenol/chloroform. Vero cells were grown to 90% confluence, trypsinized, washed twice with cold PBS, and resuspended in PBS. RNA transcripts were added to 400 μl of Vero cell suspension in an electroporation cuvette and electroporated with one pulse at 450 V, 50 μF with a Bio-Rad Gene Pulser II electroporator. The transfected Vero cells were cultured overnight in 1% FBS-containing MEM in a 60 mm dish or a six-well plate and further cultured in MEM without FBS.

Analysis of the negative strand and subgenomic RNAs by RT-PCR, real-time PCR

Total RNA was extracted from Vero cells electroporated in in vitro-synthesized transcripts after treatment with DNaseI, using TRI Reagent (Molecular Research Center, Inc.) at 24 or 48 h post-electroporation. Reverse transcription was performed with Expand Reverse Transcriptase (Roche) using equal amount of RNA. After optimization, real-time PCR was performed using LightCycler FastStart DNA Master SYBR Green I kit according to the manufacturer's instructions (Roche).

Northern blot analysis

Vero cells were infected with wild type and mutant viruses at a multiplicity of approximately 1, and total RNA was extracted from the infected cells. Ten micrograms of RNA was added to a mixture of 1× MOPS, 37% formaldehyde, and formamide and incubated at 65 °C for 20 min before subjected to gel electrophoresis. The segregated RNA bands were transferred onto a Hybond N+ membrane (Amersham Biosciences) via capillary action overnight and fixed by UV crosslinking (Stratalinker). Hybridization of Dig-labeled DNA probes was carried out at 50 °C in hybridization oven overnight. Membranes were washed 3 times for 15 min each with the probe buffer, before proceeding to detection with CDP-Star (Roche) according to the manufacturer's instructions.

Western blot analysis

Vero cells were infected with wild type and mutant viruses at a multiplicity of approximately 1. Total proteins extracted from the infected Vero cells were lysed with 2× SDS loading buffer in the presence of 200 mM DTT plus 10 mM of iodoacetamide and subjected to SDS-PAGE. Proteins were transferred to PVDF membrane (Stratagene) and blocked overnight at 4 °C in blocking buffer (5% fat free milk powder in PBST buffer). The membrane was incubated with 1:2000 diluted primary antibodies in blocking buffer for 2 h at room temperature. After washing three times with PBST, the membrane was incubated with 1:2000 diluted anti-mouse or anti-rabbit IgG antibodies conjugated with horseradish peroxidase (DAKO) in blocking buffer for 1 h at room temperature. After washing three times

with PBST, the polypeptides were detected with a chemiluminescence detection kit (ECL, Amersham Biosciences) according to the manufacturer's instructions.

Growth curve and plaque sizes of the recombinant viruses on Vero cells

Confluent monolayers of Vero cells on six-well plates were infected with 100 μl of 100-fold diluted virus stock. After 1 h of incubation at 37 °C, cells were washed twice with PBS and cultured in 3 ml of MEM containing 0.5% carboxymethy cellulose for 3 days. The cells were fixed and stained with 0.1% toluidine.

Vero cells were infected with wild type and recombinant IBV and harvested at different times post-infection. Viral stocks were prepared by freezing/thawing of the cells three times. The 50% tissue culture infection dose (TCID50) of each sample was determined by infecting five wells of Vero cells on 96-well plates in duplicate with 10-fold serial dilution of each viral stock.

Acknowledgments

This work was supported by the Agency for Science Technology and Research, Singapore, and by a grant from the Biomedical Research Council (BMRC 03/1/22/17/220), Agency for Science, Technology and Research, Singapore.

References

Almazan, F., Gonzalez, J.M., Penzes, Z., Izeta, A., Calvo, E., Plana-Duran, J., Enjuanes, L., 2000. Engineering the largest RNA virus genome as an infectious bacterial artificial chromosome. Proc. Natl. Acad. Sci. U.S.A. 97, 5516–5521.

Boursnell, M.E.G., Brown, T.D.K., Foulds, I.J., Green, P.F., Tomley, F.M., Binns, M.M., 1987. Completion of the sequence of the genome of the coronavirus avian infectious bronchitis virus. J. Gen. Virol. 68, 57–77.

Casais, R., Thiel, V., Siddell, S.G., Cavanagh, D., Britton, P., 2001. Reverse genetics system for the avian coronavirus infectious bronchitis virus. J. Virol. 75, 12359–12369.

Casais, R., Dove, B., Cavanagh, D., Britton, P., 2003. Recombinant avian infectious bronchitis virus expressing a heterologous spike gene demonstrates that the spike protein is a determinant of cell tropism. J. Virol. 77, 9084–9089.

Casais, R., Davies, M., Cavanagh, D., Britton, P., 2005. Gene 5 of the avian coronavirus infectious bronchitis virus is not essential for replication. J. Virol. 79, 8065–8078.

Coley, S.E., Lavi, E., Sawicki, S.G., Fu, L., Schelle, B., Karl, N., Siddell, S.G., Thiel, V., 2005. Recombinant mouse hepatitis virus strain A59 from cloned, full-length cDNA replicates to high titers in vitro and is fully pathogenic in vitro. J. Virol. 79, 3097–3106.

Fang, S.G., Shen, S., Tay, F.P., Liu, D.X., 2005. Selection of and recombination between minor variants lead to the adaptation of an avian coronavirus to primate cells. Biochem. Biophys. Res. Commun. 336, 417–423.

Hodgson, T., Britton, P., Cavanagh, D., 2006. Neither the RNA nor the proteins of open reading frames 3a and 3b of the coronavirus infectious bronchitis virus are essential for replication. J. Virol. 80, 296–305.

Ivanov, K.A., Thiel, V., Dobbe, J.C., van der Meer, Y., Snijder, E.J., Ziebuhr, J., 2004. Multiple enzymatic activities associated with severe acute respiratory syndrome coronavirus helicase. J. Virol. 78, 5619–5632.

Koetzner, C.A., Parker, M.M., Ricard, C.S., Sturman, L.S., Masters, P.S., 1992. Repair and mutagenesis of the genome of a deletion mutant of the coronavirus mouse hepatitis virus by targeted RNA recombination. J. Virol. 66, 1841–1848.

Lim, K.P., Liu, D.X., 1998a. Characterization of a papain-like proteinase domain encoded by ORF1a of the coronavirus IBV and determination of the C-terminal cleavage site of an 87 kDa protein. Adv. Exp. Med. Biol. 440, 173–184.

Lim, K.P., Liu, D.X., 1998b. Characterization of the two overlapping papain-like proteinase domains encoded in gene 1 of the coronavirus infectious bronchitis virus and determination of the C-terminal cleavage site of an 87 kDa protein. Virology 245, 303–312.

Lim, K.P., Ng, L.F., Liu, D.X., 2000. Identification of a novel cleavage activity of the first papain-like proteinase domain encoded by open reading frame 1a of the coronavirus avian infectious bronchitis virus and characterization of the cleavage products. J. Virol. 74, 1674–1685.

Liu, D.X., Tibbles, K.W., Cavanagh, D., Brown, T.D.K., Brierley, I., 1995. Identification, expression and processing of an 87K polypeptide encoded by ORF1a of the coronavirus infectious bronchitis virus. Virology 208, 47–54.

Liu, D.X., Xu, H.Y., Brown, T.D.K., 1997. Proteolytic processing of the coronavirus infectious bronchitis virus 1a polyprotein: identification of a 10 kDa polypeptide and determination of its cleavage sites. J. Virol. 71, 1814–1820.

Liu, D.X., Shen, S., Xu, H.Y., Wang, S.F., 1998. Proteolytic mapping of the coronavirus infectious bronchitis virus 1b polyprotein: evidence for the presence of four cleavage sites of the 3C-like proteinase and identification of two novel cleavage products. Virology 246, 288–297.

Marra, M.A., Jones, S.J.M., Astell, C.R., Holt, R.A., Brooks-Wilson, A., Butterfield, Y.S.N., Khattra, J., Asano, J.K., et al., 2003. The genome sequence of the SARS-associated coronavirus. Science 300, 1399–1404.

Masters, P.S., Rottier, P.J., 2005. Coronavirus reverse genetics by targeted RNA recombination. Curr. Top. Microbiol. Immunol. 287, 133–159.

Ng, L.F., Liu, D.X., 1998. Identification of a 24 kDa polypeptide processed from the coronavirus infectious bronchitis virus 1a polyprotein by the 3C-like proteinase and determination of its cleavage sites. Virology 243, 388–395.

Ng, L.F., Liu, D.X., 2000. Further characterization of the coronavirus infectious bronchitis virus 3C-like proteinase and determination of a new cleavage. Virology 272, 27–39.

Ng, L.F., Liu, D.X., 2002. Membrane association and dimerization of a cysteine-rich, 16-kDa polypeptide released from the C-terminal region of the coronavirus infectious bronchitis virus 1a polyprotein. J. Virol. 76, 6257–6267.

Rota, P.A., Oberste, M.S., Monroe, S.S., Nix, W.A., Campagnoli, R., Icenogle, J.P., Penaranda, S., et al., 2003. Characterization of a novel coronavirus associated with severe acute respiratory syndrome. Science 300, 1394–1999.

Sanchez, C.M., Izeta, A., Sanchez-Morgado, J.M., Alonso, S., Sola, I., Balasch, M., Plana-Duran, J., Enjuanes, L., 1999. Targeted recombination demonstrates that the spike gene of transmissible gastroenteritis coronavirus is a determinant of its enteric tropism and virulence. J. Virol. 73, 7607–7618.

Seybert, A., Posthuma, C.C., van Dinten, L.C., Snijder, E.J., Gorbalenya, A.E., Ziebuhr, J., 2005. A complex zinc finger controls the enzymatic activities of nidovirus helicases. J. Virol. 79, 696–704.

Shen, S., Wen, Z.L., Liu, D.X., 2003. Emergence of an avian coronavirus infectious bronchitis virus (IBV) mutant with a truncated 3b gene: functional characterization of the 3b gene in pathogenesis and replication. Virology 311, 16–27.

Shen, S., Law, Y.C., Liu, D.X., 2004. A Single amino acid mutation in the spike protein of coronavirus infectious bronchitis virus hampers its maturation and incorporation into virions at the nonpermissive temperature. Virology 326, 288–298.

Thiel, V., Herold, J., Schelle, B., Siddell, S.G., 2001. Infectious RNA transcribed in vitro from a cDNA copy of the human coronavirus genome cloned in vaccinia virus. J. Gen. Virol. 82, 1273–1281.

van Dinten, L.C., den Boon, J.A., Wassenaar, A.L., Spaan, W.J., Snijder, E.J., 1997. An infectious arterivirus cDNA clone: identification of a replicase point mutation that abolishes discontinuous mRNA transcription. Proc. Natl. Acad. Sci. U.S.A. 94, 991–996.

van Dinten, L.C., van Tol, H., Gorbalenya, A.E., Snijder, E.J., 2000. The predicted metal-binding region of the arterivirus helicase protein is involved in subgenomic mRNA synthesis, genome replication, and virion biogenesis. J. Virol. 74, 5213–5223.

Xu, H.Y., Lim, K.P., Shen, S., Liu, D.X., 2001. Further identification and characterization of novel intermediate and mature cleavage products released from the ORF 1b region of the avian coronavirus infectious bronchitis virus 1a/1b polyprotein. Virology 288, 212–222.

Youn, S., Collisson, E.W., Machamer, C.E., 2005a. Contribution of trafficking signals in the cytoplasmic tail of the infectious bronchitis virus spike protein to virus infection. J. Virol. 79, 13209–13217.

Youn, S., Leibowitz, J.L., Collisson, E.W., 2005b. In vitro assembled, recombinant infectious bronchitis viruses demonstrate that the 5a open reading frame is not essential for replication. Virology 332, 206–215.

Yount, B., Curtis, K.M., Baric, R.S., 2000. Strategy for systematic assembly of large RNA and DNA genomes: transmissible gastroenteritis virus model. J. Virol. 74, 10600–10611.

Yount, B., Denison, M.R., Weiss, S.R., Baric, R.S., 2002. Systematic assembly of a full-length infectious cDNA of mouse hepatitis virus strain A59. J. Virol. 76, 11065–11078.

Yount, B., Curtis, K.M., Fritz, E.A., Hensley, L.E., Jahrling, P.B., Prentice, E., Denison, M.R., Geisbert, T.W., Baric, R.S., 2003. Reverse genetics with a full-length infectious cDNA of severe acute respiratory syndrome coronavirus. Proc. Natl. Acad. Sci. U.S.A. 100, 12995–13000.

Yount, B., Roberts, R.S., Sims, A.C., Deming, D., Frieman, M.B., Sparks, J., Denison, M.R., Davis, N., Baric, R.S., 2005. Severe acute respiratory syndrome coronavirus group-specific open reading frames encode nonessential functions for replication in cell cultures and mice. J. Virol. 79, 14909–14922.